Computational study of irrational rotations via exact discontinuity tracking

Hannah Kravitz *

November 19, 2025

Abstract

The discrepancy sum $D_N(x,\rho)$ for irrational rotations has been of interest to mathematicians for over a century. While historically studied in an "almost-everywhere" or asymptotic sense, D_N for finite N is increasingly an object of interest for its highly nontrivial properties that depend on the Diophantine properties of ρ . This behavior is typically periodic in N with respect to the quotients of the continued fraction convergents, which can grow quite quickly for some irrationals. Thus the stable computation of the sum is necessary for forming conjectures about particular properties. However, computing the exact value of the sum and its corresponding probability density function (pdf) is notoriously difficult due to numerical instability inherent in the sum itself and the failure of sampling methods to capture the structure of its jump discontinuities. This paper presents a novel computational algorithm that fully defines the discrepancy function and its associated pdf through its discontinuities. This allows the calculation of $D_N(x,\rho)$ to machine precision with minimal storage in O(N) time. This vast improvement in computability over the $O(N^2)$ naive version enables, for the first time, the direct computation of the exact pdf up to machine precision in $O(N \log N)$ time, and with it, some key properties of the discrepancy: $||D_N||_{\infty}$ (half of the support of the pdf), $||D_N||_2^2$ (the variance of the pdf), and the kurtosis of the pdf. A key strength of the discontinuity-tracking algorithm lies in its ability to produce clear, exact figures, allowing the development of mathematical intuition and the quick testing of conjectures. As an example, a newly conjectured pattern is presented: when ρ is well-approximated by rational $\frac{p_n}{q_n}$, the pdf exhibits a predictable spiked-trapezoidal pattern when $N=kq_n$. These shapes degrade eventually as k increases, with the degradation speed depending on how well $\frac{p_n}{q_n}$ approximates ρ .

1 Introduction

The study of uniform distribution modulo one is a classic topic in number theory. A key object of interest is the discrepancy sum for a rotation, defined as

$$D_N(x,\rho) = \sum_{k=1}^{N} \left[(x+k\rho) \mod 1 - \frac{1}{2} \right].$$
 (1)

with $x \in [0,1)$, ρ (typically irrational) $\in [0,1)$, and $N \in \mathbb{N}$. D_N , a particular example of a Birkhoff sum, quantifies deviations of the sequence's average from its expected mean of $\frac{1}{2}$ [2,16]. Theoretical work spanning nearly a century has analyzed the growth rates, extrema, asymptotic behavior, and other properties of $D_N(x,\rho)$ (see, for example, [1,4,8,14–16,18,20–22,24,25,27–29]) yet many questions still remain unanswered.

^{*}hkravitz@pdx.edu

A primary reason for this enduring interest is that this simple function exhibits highly complex self-similar patterns that evolve and change, determined by the Diophantine properties of ρ and the choice of N. However, these features grow finer as N increases, making them difficult to resolve computationally using standard methods. This creates a significant barrier to using numerical exploration for testing conjectures. Furthermore, the theoretical literature on this topic is often presented without figures, obscuring the fascinating geometric patterns the mathematics reveal.

The computational challenges are threefold:

- First, the naive summation in Equation 1 is notoriously prone to numerical instability; the repeated use of the mod 1 operation on large terms runs a high risk of catastrophic cancellation (loss of nearly all significant digits from subtracting two nearby numbers) [6, 12].
- Second, the function's structure consists of up to N branches with jump discontinuities. For irrational ρ , a uniform sampling of $x \in [0,1)$ is guaranteed to miss the branch endpoints, which are fundamental to the structure of the probability density function (pdf). As N varies, D_N presents intricate fine-scale features for irrational ρ that sampling is also nearly guaranteed to miss, like very short branches and branches that are nearly (but never exactly) aligned.
- Third, resolving this complex structure to even roughly discern some features is computationally prohibitive itself, requiring $O(N^2)$ time and $O(N^2)$ storage. This makes even familiar rotation numbers like $\rho = \pi 3$ difficult to study, as the most interesting behavior typically occurs when N is a multiple of the denominator of a continued fraction convergent; the fourth such partial quotient for $\pi 3$ is N = 33, 102.

In this paper, we overcome all three of these barriers by introducing an efficient and stable algorithm that computes the discrepancy function D_N exactly, to machine precision. By developing a novel method to track the N discontinuities directly, our algorithm achieves what was unattainable using naive sampling: it runs in O(N) time, operates with machine precision (bypassing the numerical instabilities inherent in the summation and avoiding large sampling errors), and requires only O(N) storage.

A direct consequence of this algorithm is the ability to exactly compute the probability density function (pdf) associated with $D_N(x,\rho)$ in $O(N\log N)$ time, with O(N) storage, at machine precision. This new computation enables, for the first time, the exact calculation of the fundamental statistical properties of the pdf: $||D_N||_{\infty}$ (half of the support of the pdf), $||D_N||_2^2$ (the variance of pdf), the kurtosis. It also allows the rapid generation of highly accurate figures to help guide mathematical intuition.

1.1 Discrepancy

Equation 1 may be rewritten in a form more stable to double-precision arithmetic errors:

$$D_N(x,\rho) = Nx + \frac{N(N+1)}{2}\rho - \frac{N}{2} - \sum_{k=1}^{N} \lfloor x + k\rho \rfloor$$
 (2)

where $\lfloor \cdot \rfloor$ is the floor function. This formulation also reveals the structure of D_N as piecewise-linear with branches of slope N. For irrational ρ , the jumps between segments caused by the floor function will have height exactly 1, while the length of the segments vary. As N increases, the plots of D_N reveal a self-similar structure with intricacies determined by the Diophantine properties of ρ .

Figure 1 shows
$$D_N$$
 for $\rho = L = \sum_{k=1}^{\infty} \frac{1}{10^{k!}} \approx 0.110001000000000$, Liouville's constant for several

N to show both the capabilities of the algorithm and the behavior of the function. The first row shows very short branches, even for small N. As N increases in the second and third rows, a self-similar structure emerges, with branches grouped in blocks with periodic properties.

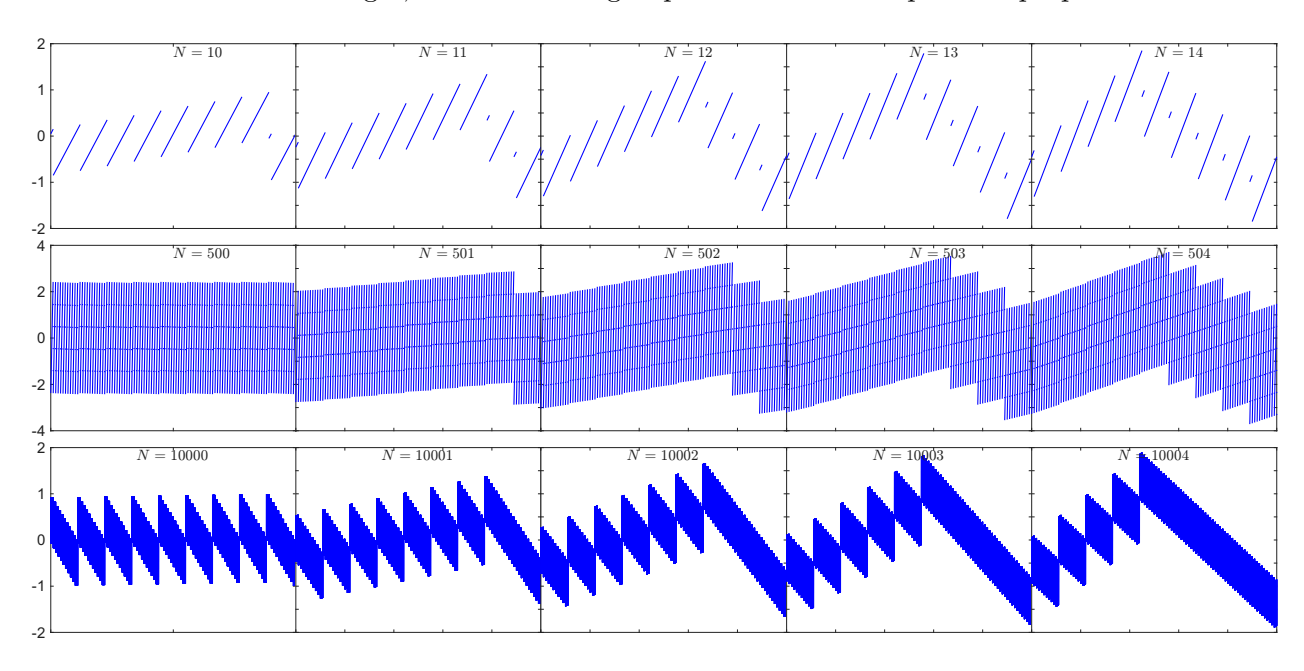


Figure 1: This figure shows the plot of $D_N(x,L)$ for different N. The three rows show different levels of a self-similar structure changing with N.

1.2 Probability density function and its statistical properties

We find the probability density function pdf(y) using the standard formula for a non-monotonic transformation on a uniform distribution [19], in this case $D_N(x, \rho) : [0, 1) \to \mathbb{R}$, with ρ fixed:

$$pdf(y) = \sum_{x \in D_N^{-1}(y)} \frac{1}{|D_N'(x,\rho)|} = \sum_{x \in D_N^{-1}(y)} \frac{1}{N} = \frac{\#\{x \in D_N^{-1}(y)\}}{N}$$
(3)

where $D_N^{-1}(y)$ is the preimage of y and $\#\{\cdot\}$ is the cardinality of a set. The structure of pdf(y) is piecewise-constant, with segments becoming extremely short as N grows large.

While this distribution is often studied in the context of ergodic theory, i.e. "almost everywhere" and asymptotic results, highly structured and nontrivial behaviors occur for particular ρ and N combinations. These patterns, which our algorithm computes with machine precision for the first time, are directly governed by the Diophantine approximation properties of ρ . A few different pattern types are shown in Figures 2 and 3. The left panels of the two figures shows the distributions, while the right panels shows a zoomed-in version, showing the detail that statistical sampling would be guaranteed to miss.

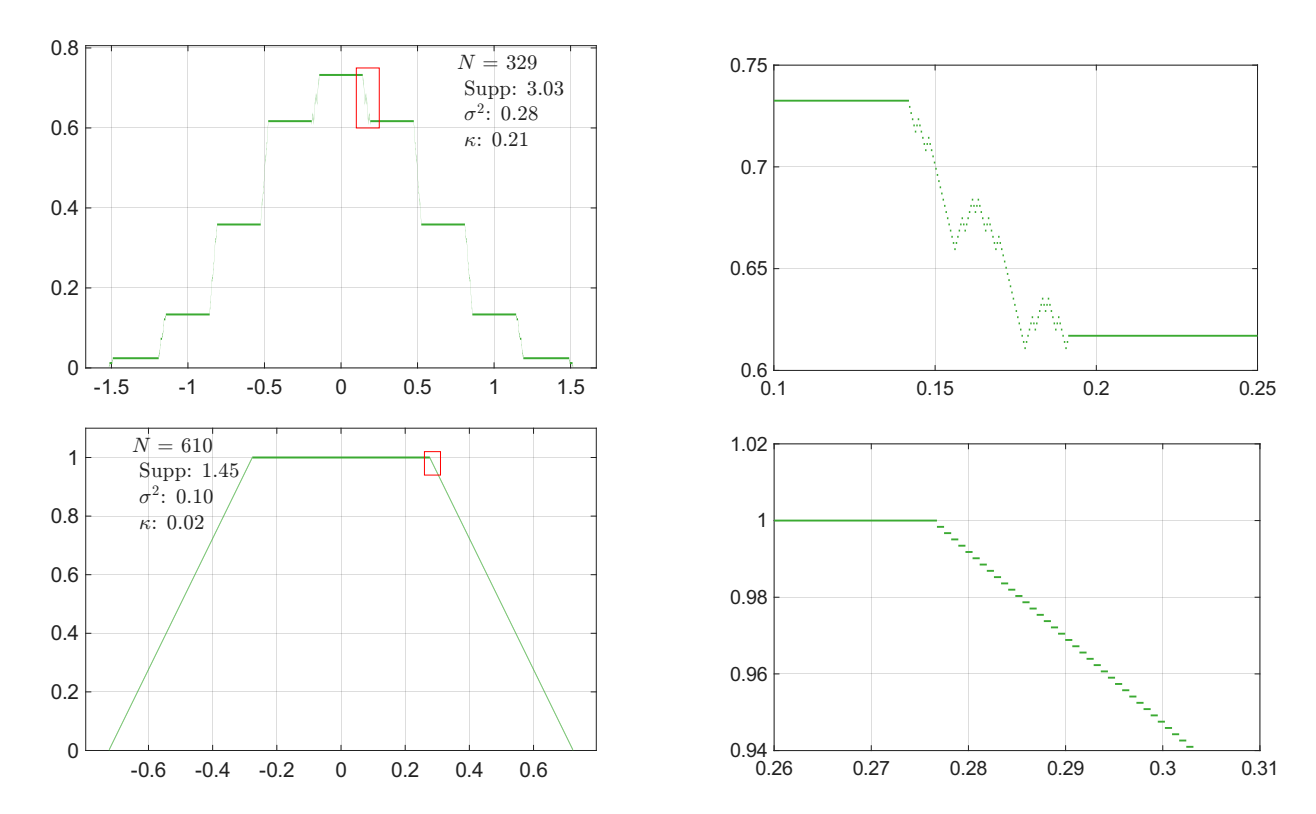


Figure 2: (Left) pdf for $\rho = \frac{\sqrt{5}-1}{2}$ (the golden ratio) for two choices of N. The top, N=329, shows a few straight platforms connected by very short segments of varying heights, while N=610 (a partial quotient for ρ) has a long straight horizontal line at y=1, indicating that all branches pass through a particular range of values containing zero, with piecewise-constant line segments making up the sides of this trapezoid-like distribution. (Right) The pdf functions are zoomed in to show the detail the algorithm is able to capture.

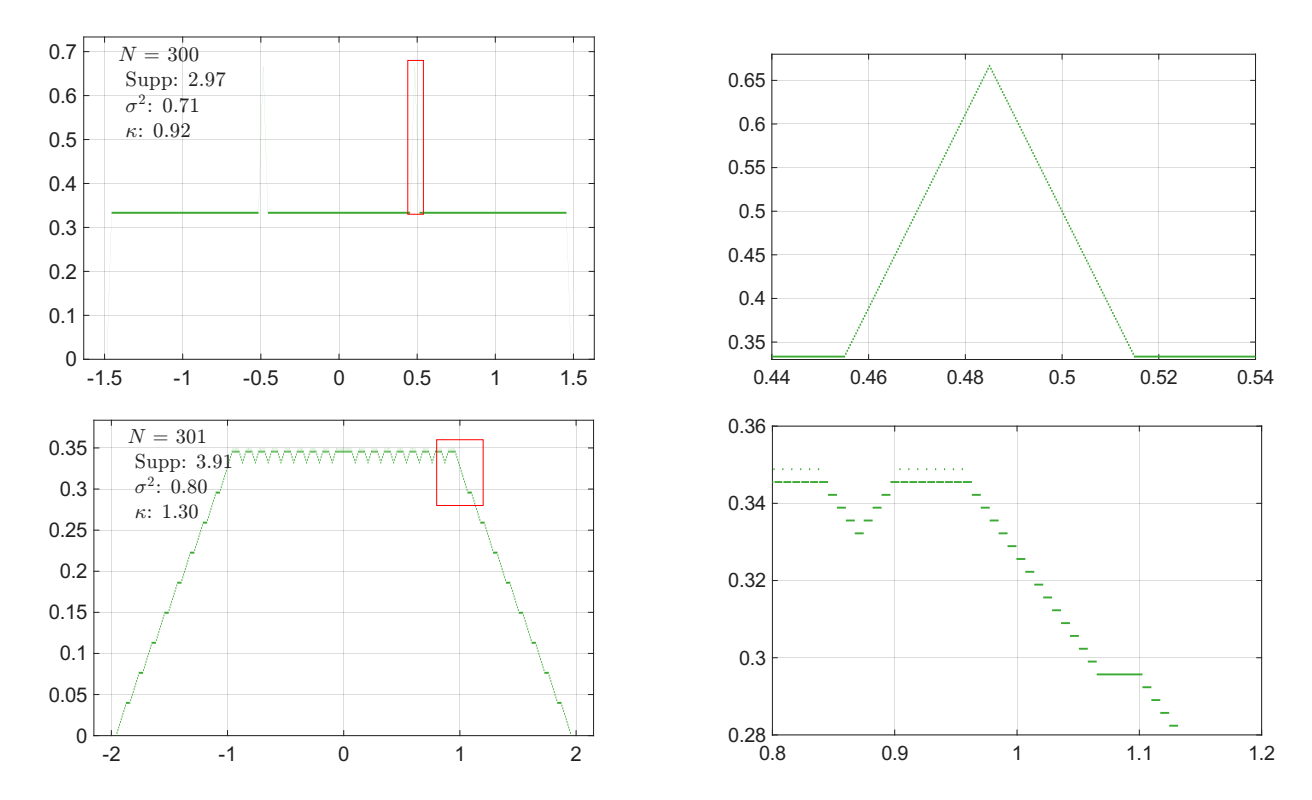


Figure 3: (Left) pdf for $\rho = L$ (Liouville's constant). Two consecutive values of N are shown, N = 300, a multiple of the second convergent denominator, and N = 301, where the support of the distribution immediately spreads out. (Right) The pdf functions are zoomed in to show the detail the algorithm is able to capture.

1.2.1 Descriptive statistics

We now introduce the descriptive statistics of pdf(y) that can now be computed directly, while also noting their interpretation in terms of the discrepancy function D_N . The descriptive statistics for particular pdfs are indicated in Figures 2 and 3.

- Support, Supp(pdf). The support of pdf(y) is the interval $[\min(D_N), \sup(D_N)]$. Due to the symmetry of the distribution, $||D_N||_{\infty} = \sup_x D_N(x, \rho) = -\min_x D_N(x, \rho)$. Our algorithm also directly computes the previously-inaccessible x-locations of the jump-discontinuities where these extrema occur.
- Variance, σ^2 , given by $E[Y^2] E[Y]^2$ where E is the expected value [5]. Since the mean of our distribution is zero, we apply the definition of the variance of a random variable Y and then the Law of the Unconscious Statistician [5], noting that [0,1) has a uniform probability density function:

$$\sigma^2 = E[Y^2] = \int_{-\infty}^{\infty} y^2 \operatorname{pdf}(y) \, dy = \int_0^1 \left(D_N(x, \rho) \right)^2 \cdot 1 \, dx = ||D_N||_2^2. \tag{4}$$

• **Kurtosis**, κ , is a measure of "tailedness" of a function, with a Gaussian having kurtosis of 3 [5]:

$$\kappa = \frac{E[Y^4]}{\sigma^4} = \frac{1}{\sigma^4} \int_{-\infty}^{\infty} y^4 \operatorname{pdf}(y) \, dy. \tag{5}$$

These statistics as a function of N are shown in Appendix A for several ρ .

2 Numerical implementation

Several authors have studied D_N or related objects numerically, typically focusing on particular quantities or specific subsequences of N. For example, Setokuchi computes $D_N(0,\rho)$ for N up to 10^7 by sampling N every 10 points [24], while Mori, Shimaru, & Takashima sampled multiples of partial quotients [18]. An investigation of $D_N(x,\rho)$ for particular N and ρ was conducted by Bountis, Veerman, & Vivaldi by sampling x [4], and a similar sampling-based strategy was employed by Vinson in the study of a related function [33]. Methods based on sampling the domain tend to be very slow and present difficulties in distinguishing mathematical behavior from numerical artifacts (see Section 2.1). Other numerical work considers weighted versions of Equation 1, often in the Fourier domain [3, 7, 9–11]. In contrast, our focus is resolving the fine spatial structure of D_N itself, enabling both D_N , its pdf, and the associated statistics to be studied with exact, rather than sampled, information.

2.1 Naive algorithm

To establish a baseline for comparison, we first consider the naive algorithm (Algorithm 1), which directly implements Equation 1 by sampling N_{samples} points across an interval $x \in [0, 1)$.

```
Algorithm 1 Naive algorithm for D_N
```

```
 \begin{array}{lll} \textbf{Require:} & N \in \mathbb{N}, \ \rho \in [0,1), \ \texttt{Nsamples} \in \mathbb{N} \\ & \texttt{xlist} \leftarrow \texttt{linspace}(0,1,\texttt{Nsamples}) \\ & \texttt{Slist} \leftarrow \texttt{zeros}(1,\texttt{Nsamples}) \\ & \textbf{for} \ k \leftarrow 1 : \texttt{len}(\texttt{xlist}) \ \textbf{do} \\ & S \leftarrow 0 \\ & \textbf{for} \ i \leftarrow 1 : N \ \textbf{do} \\ & S \leftarrow S + \ \texttt{mod}(\texttt{xlist}[k] + i\rho, 1) - \frac{1}{2} \\ & \textbf{end for} \\ & \texttt{Slist}[k] \leftarrow S \\ & \textbf{end for} \\ \end{array}
```

As discussed in Section 1, the repeated modular arithmetic produces imprecise results, sampling and storage are both $O(N^2)$, and the sampled points are statistically guaranteed to miss the key features of D_N .

2.2 Discontinuity-tracking algorithm

To overcome the fundamental limitations of sampling, we present a discontinuity-tracking algorithm (we use DTA for short) to exactly compute $D_N(x,\rho)$ with errors as low as possible, on the order of machine epsilon. We first consider the structure of the equivalent expression for D_N , reproduced here for convenience:

$$D_N(x,\rho) = Nx + \frac{N(N+1)}{2}\rho - \frac{N}{2} - \sum_{k=1}^{N} \lfloor x + k\rho \rfloor.$$

Where the naive implementation of modular arithmetic suffers from catastrophic cancellation, the floor function $\lfloor y \rfloor$ results in an exact integer. The expression $\frac{N(N+1)}{2}$, which multiplies ρ is also an exact integer for practical N (that is, $N < 2^{53}$); multiplying by ρ last keeps the arithmetic in the integer regime for as long as possible.

The main innovation in the DTA is in noticing that D_N is piecewise-linear with branches of slope N and therefore fully defined by its branch endpoints; thus we significantly reduce both the computational and storage load by computing only those points. Jump discontinuities occur at $x = \lceil k\rho \rceil - k\rho$, where $\lceil \cdot \rceil$ represents the ceiling function. This computation for x may introduce some catastrophic cancellation, but it is important to note that these errors **do not accumulate**, as each x is independent of the next. The cancellation error may be mitigated by a careful application of the Steinhaus conjecture (three-gap theorem) [31] by noting that there are at most three distinct distances between consecutive points, but we leave that as a direction for future work.

Another important insight is noticing that the jumps must always be of integer height, and of height 1 for irrational ρ . The algorithm identifies and stores discontinuities within [0,1), preserving duplicates in the rational case to track the height of the jumps. First, the y-intercept, $D_N(0,\rho)$, is computed. Then, the differences between successive discontinuities (Δx) determine branch widths along the x-axis. r duplicate discontinuities indicate a jump of height r. D_N can then be fully characterized by leveraging the slopes N and branch widths Δx . Minimal storage is required, as the only values that need to be stored are the branch endpoints. Algorithm 2 provides a detailed implementation of this approach.

Algorithm 2 Discontinuity-tracking algorithm

```
Require: N \in \mathbb{N}, \rho \in [0, 1)

1: disc_list = \{\lceil k\rho \rceil - k\rho\} \cap [0, 1)  \triangleright Identify locations of discontinuities

2: disc_list = sort(disc_list, ascending)

3: Create \Delta x_{\text{list}} = \text{diff (disc_list)}  \triangleright find the difference between consecutive terms

4: D_N(0, \rho) = \frac{N(N+1)}{2}\rho - \frac{N}{2} - \sum_{k=1}^{N} \lfloor k\rho \rfloor  \triangleright Compute y-intercept

5: a_1 \leftarrow D_N(0, \rho) and b_1 \leftarrow a_1 + N\Delta x_{\text{list}}[1]. \triangleright 1st branch spans y \in [a_1, b_1)

6: for j = 2 to len(disc_list) do

7: Set a_j = b_{j-1} - 1 and b_j = a_j + N\Delta x_{\text{list}}[j]. \triangleright kth branch spans y \in [a_k, b_k)

8: Corresponding x-values are (disc_list[j-1], disc_list[j])

9: end for
```

To quantify the efficiency of the improved algorithm, we first determine the number of floating point operations (FLOPs) required. Consider the y-intercept of $D_N(x, \rho)$:

$$D_N(0, \rho) = \frac{N(N+1)}{2}\rho - \frac{N}{2} - \sum_{k=1}^{N} \lfloor k\rho \rfloor.$$

Computing the sum $\sum_{k=1}^{N} \lfloor k\rho \rfloor$ requires N multiplications and N-1 additions, totaling 2N-1 operations. Adding the remaining terms contribute seven additional operations, yielding a total of 2N+6.

Each discontinuity occurs at $x = \lceil k\rho \rceil - k\rho$, requiring three operations per discontinuity. With at most N discontinuities, this adds 3N operations. The endpoints of each branch are computed via $b_j = a_j + N\Delta x[j]$ (two operations) and $a_j = b_{j-1} - 1$ (one operation), adding another 3N operations. Defining the full structure of $D_N(x,\rho)$ thus requires only 8N + 6 operations.

The overall order of the algorithm will depend on the choice of sorting algorithm. Our benchmarking in Section 3 was performed in MATLAB [30]; its sort function runs in O(N) time, using a combination of binning and Quicksort [17]. Quicksort runs in $O(m \log(m))$ time for each bin [23], but when run on the smaller bins of size $m \ll N$, the time contribution is mostly negligible. Therefore, the order of the algorithm is, with proper choice of sorting algorithm, O(N).

2.3 Exact implementation of the pdf

The DTA (Algorithm 2) provides an exact definition of the branch start and endpoints, $\{a_i\}$ and $\{b_i\}$ respectively. This collection of 2N+2 points (may be fewer for rational ρ , depending on N) partitions the range of $D_N(x,\rho)$ into bins. Then we just count the branches that fall into each bin. This count may be accomplished through an implementation of the sweep line method which is $\mathbf{O}(\mathbf{N}\log(\mathbf{N}))$ [26]. A naive implementation in which every interval is checked against every segment would be $O(N^2)$.

The statistical measures of pdf(y), closely related to the L^p -norms of D_N , are typically studied in the context of their growth as a function of N. Thus, efficient algorithms are of utmost importance for a feasible study.

Support

The extrema of D_N , which define the support of pdf are easily found using built-in max/min functions. $||D_N||_{\infty}$ is equal to $\sup_x |D_N(x,\rho)|$.

Variance

The variance, as given in Equation 4 can be easily simplified into an exact discrete equation by considering both the piecewise-constant structure of pdf(y) and its compact support. Thus, we have

$$\sigma^2 = \int_{-\infty}^{\infty} y^2 \operatorname{pdf}(y) \, dy = \sum_{j=1}^{m} \frac{c_j}{3} \left(y_{j+1}^3 - y_j^3 \right) \tag{6}$$

where m is the number of piecewise-constant line segments, c_j is the constant value of pdf(y) on the segment, and y_j and y_{j+1} are the starting and ending y-values of that segment, respectively. $\sigma^2 = ||D_N||_2^2$ as established in Equation 4. This computation is $\mathbf{O}(\mathbf{N})$.

Kurtosis

Kurtosis, as given in Equation 5 can be computed in a similar manner to the variance:

$$\kappa = \frac{1}{\sigma^4} \int_{-\infty}^{\infty} y^4 \operatorname{pdf}(y) \, dy = \frac{1}{\sigma^4} \sum_{j=1}^m \frac{c_j}{5} \left(y_{j+1}^5 - y_j^5 \right). \tag{7}$$

Using the variance σ^2 previously computed, this computation is $\mathbf{O}(\mathbf{N})$.

3 Algorithm benchmarking

In Section 2, we showed that our algorithm was correct on the order of machine epsilon, i.e. the maximum error in $D_N(x,\rho)$ is $O(N\varepsilon_{\text{mach}})$, and runs in O(N) time. Now we must show that these claims hold in practical application. All tests are run in MATLAB R2025b [30].

3.1 Time complexity

The naive method samples $D_N(x, \rho)$ at some subset of points in [0, 1). As discussed in Section 2.1, uniform sampling is unable to fully resolve the function, so for the purposes of making a time comparison, we take a very sparse sample: N points uniform in [0, 1). Figure 4 shows runtime

results for $\rho = \frac{\sqrt{5}-1}{2}$ for the naive algorithm (Algorithm 1), its vectorized version, and the DTA (Algorithm 2). The left panel confirms that the naive algorithm is $O(N^2)$, improved to $O(N^{1.75})$ through vectorization. The right panel shows that the DTA runs in $\mathbf{O}(\mathbf{N})$ time (represented by a linear fit with slope of 1 and $R^2 = 0.97$). Similar results hold across choices of ρ ; the same analysis was run with $\rho = L$ (slope of 1.07, $R^2 = 0.97$).

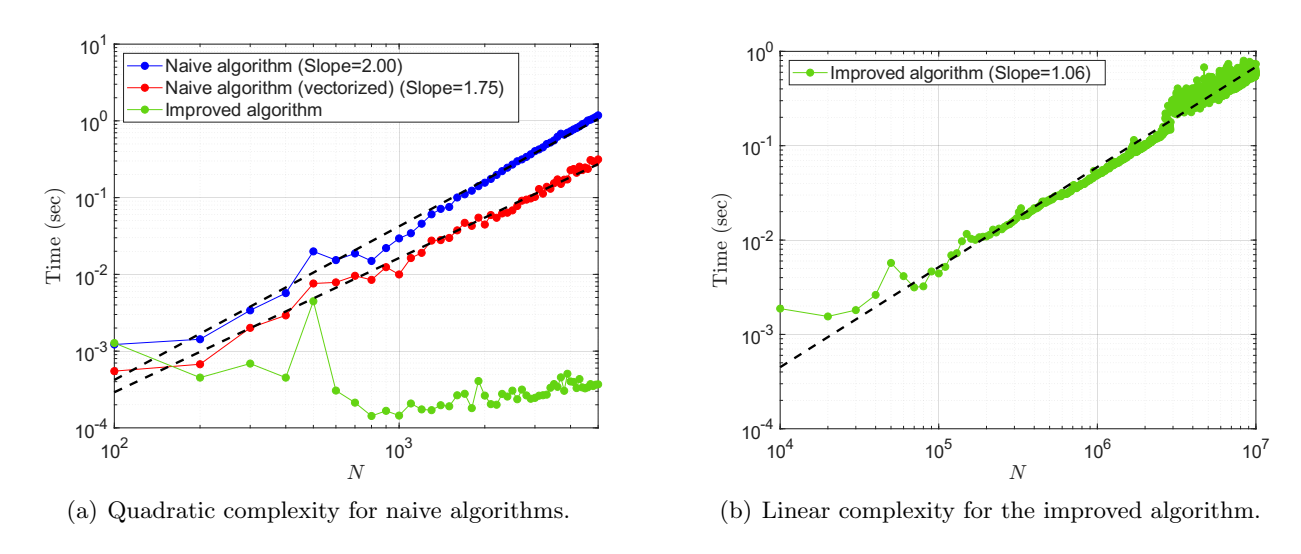


Figure 4: Comparison of time complexities for the algorithms.

3.2 Error analysis

For rational ρ , D_N exhibits a predictable structure for particular N. When $\rho = \frac{p}{q}$ and N = kq, D_N forms q branches spanning $[-\frac{k}{2}, \frac{k}{2}]$ and $x \in [\frac{r-1}{q}, \frac{r}{q}]$ for $r = 1, 2, \ldots, q$ (Changing p does not change the behavior for N = kq). Vertical jumps of height k occur between branches. To evaluate the accuracy of the algorithm, we set $\rho = \frac{1}{q}$ and N = q. The infinity norm of the error is the maximal endpoint deviation from $\pm \frac{1}{2}$. Results in Figure 5 show that errors in D_N grow proportionally to $\frac{1}{2}N\varepsilon_{\rm mach}$, as confirmed by a linear fit with $R^2 = 0.95$. Errors are exactly zero for $q = 2^j$, $j \in \mathbb{N}$, corresponding to ρ values exactly representable in double-precision. Of course these zero errors can only be a feature of rational ρ .

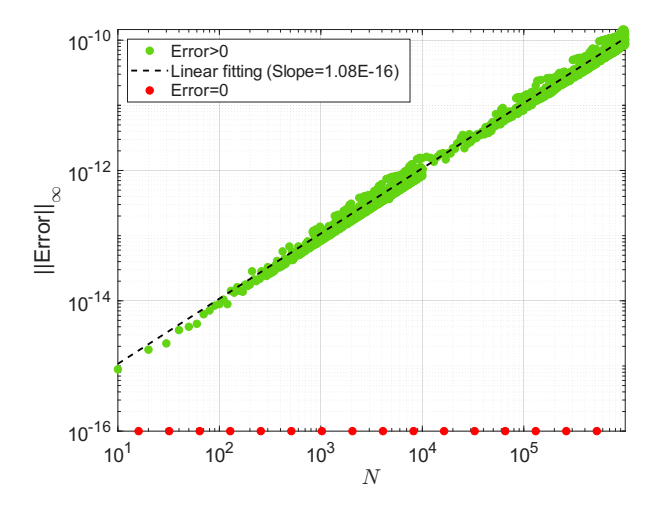


Figure 5: The maximum error (∞ -norm) of the algorithm grows with the number of terms as $\frac{1}{2}\varepsilon_{\text{mach}}$.

4 Discussion

The improved algorithm overcomes the $O(N^2)$ computational barrier, and the numerical stability barriers, bringing the study of the discrepancy of irrational rotations firmly into the regime of experimental mathematics for the first time. We now present some examples of what can be studied using this tool. We focus on the support of the discrepancy, $\operatorname{Supp}(\operatorname{pdf})$ (half of $||D_N||_{\infty}$), as it is the most common metric in the theoretical literature. The variance (equivalently, $||D_N||_2^2$) and kurtosis exhibit behavior highly correlated with $||D_N||_{\infty}$, as all three metrics respond to the branch realignments in related ways, e.g. have local extrema at partial quotients and exhibit self similarity with respect to multiples of these quotients (see Appendix A).

4.1 Self-similar patterns in the support of D_N

It is a foundational result in number theory that the behavior of $D_N(x,\rho)$ is governed by the partial quotients of ρ ; in particular, local minima occur when $N=q_n$ is a partial quotient of ρ [16]. Therefore, in order to capture the structure of $D_N(x,\rho)$ as N increases without sampling too many N, we use the partial quotients and their multiples as anchors and sample logarithmically between them. In order to find the local maxima numerically, a different sampling strategy would be required.

Figure 6 shows Supp(pdf) on a log-log plot for a few classes of irrationals, with the partial quotients plotted as red dots. Various types of self-similarity can be observed. The top row shows $\rho = L$ (Liouville's constant) and $\rho = \pi$, whose support functions in this regime are characterized by a very large hills preceding the large partial quotient (9,909 for L and 33,102 for π), as observed by Vinson [33] for $\rho = \pi$ and by Shimaru & Takashima [28] and Setokuchi & Takashima [25] for quadratic irrationals with similar properties. The second row shows two transcendentals without particularly high partial quotients, $\rho = e - 2$ and $\rho = \frac{\pi^2}{6} - 1$. The last row shows two quadratic irrationals, which are characterized by eventually-repeating partial fraction representations. $\rho = \sqrt{2} = [2, 2, \ldots]$ cannot sustain large peaks due to the regularity its partial quotients. $\rho = \alpha_{ST} = [2, 40, 40, 2, 2, \ldots]$, a quadratic irrational studied by Shimaru & Takashima [28], has some large early hills then settles into a more regular structure without large peaks.

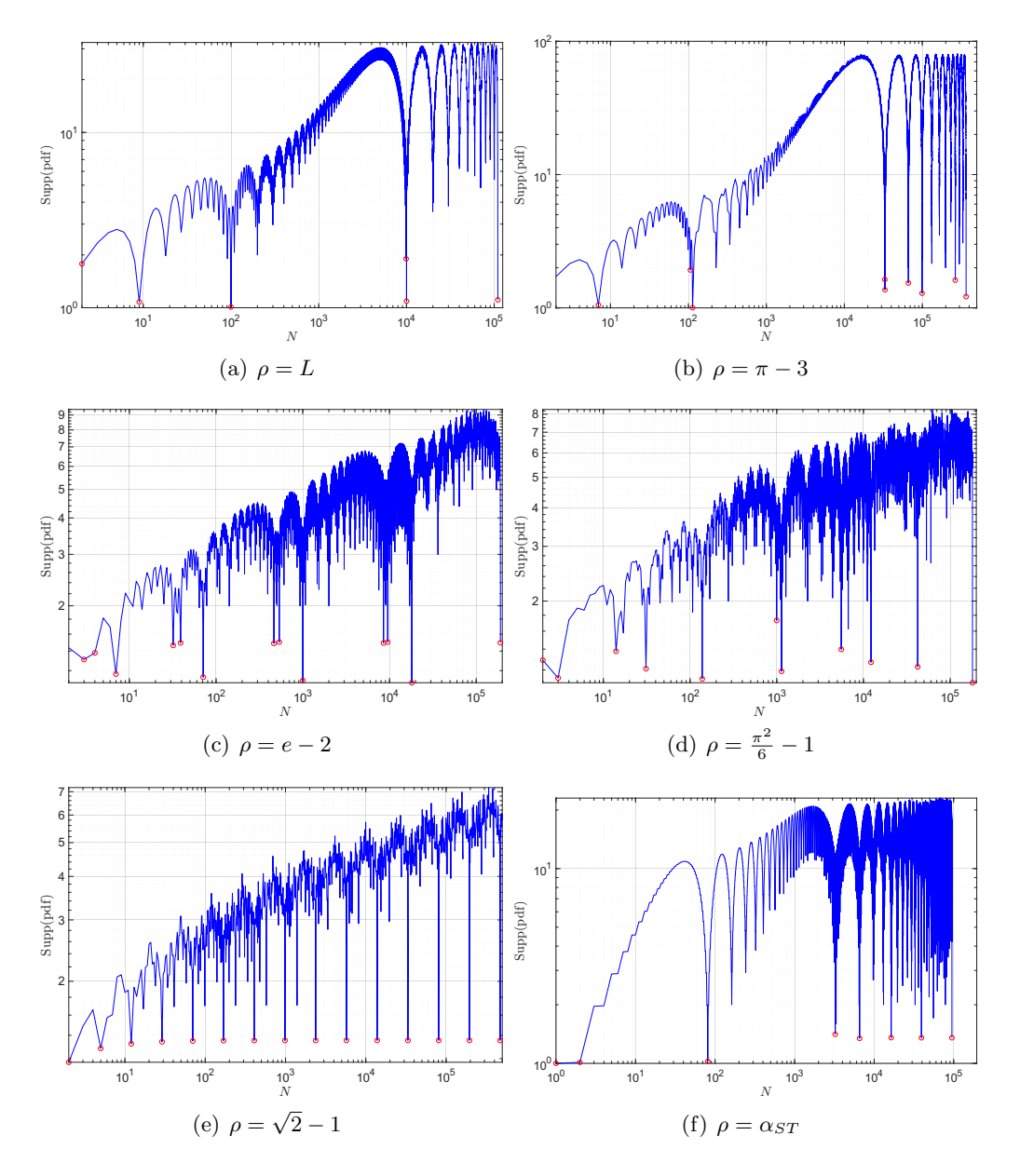


Figure 6: Plots of Supp(pdf(y)) for various classes of irrational numbers for $N=2,3,\ldots$, with the partial quotients plotted in red. (Top row) Transcendental numbers with a large partial quotient. (Second row) Transcendental numbers with a medium-sized partial quotient. (Third row) Quadratic irrationals: on the left is $\sqrt{2} = [2,2,\ldots]$, and on the right is $\alpha_{ST} = [2,40,40,2,2,\ldots]$ studied by Shimaru & Takashima [28].

4.2 Recurring patterns in the pdf

Trapezoids

As discussed in the previous section, $||D_N(x,\rho)||_{\infty}$ (half of $\operatorname{Supp}(pdf)$) is minimal when $N=q_n$ is a partial quotient [16]. These are the points where ρ is best approximated by a rational number $\frac{p_n}{q_n}$. This manifests in the plot of D_N as branches that are highly aligned. An earlier version of this algorithm developed by the present author was used by Veerman, Ralston, Tangerman, &

Wu to provide supporting numerical evidence for their "trapezoid theorem," which states that this alignment causes the pdf to reach its maximum possible height of 1 if and only if $N = q_n$ [32].

Here we provide some brief geometric intuition for the theorem. For rational $\rho = \frac{p}{q}$ with N = q, D_N forms q perfectly aligned branches spanning $\left[-\frac{1}{2},\frac{1}{2}\right]$. The corresponding pdf is the rectangular uniform distribution $\left[-\frac{1}{2},\frac{1}{2}\right]\times [0,1]$. The trapezoid theorem asserts that when ρ is irrational and $N=q_n$ is a convergent denominator, D_N is characterized by q_n branches, all of which overlap on a smaller subset of $\left[-\frac{1}{2},\frac{1}{2}\right]$, with some shifted a bit on either end. The height still reaches 1, but the length of the top is now shorter than 1. This causes the base to widen, as the pdf is a distribution and its area must always equal 1. The result is a trapezoid whose dimensions depend on the quality of the rational approximation $\frac{p_n}{q_n}$ to ρ . The shape is not a "true" trapezoid in that the sides are made up of small piecewise constant line segments.

Trapezoids with spikes

Numerical experiments show particular patterns for ρ when it is **well-approximated** by rational $\frac{p_n}{q_n}$ and $N=kq_n$ for $k=1,2,\ldots m$. In this case, we see the distribution develop k-1 spikes, starting from the center. The area between the spikes remains completely flat until a particular m when the shape begins to degenerate into oscillatory noise. How quickly this degeneration happens depends on how well-approximated ρ is by $\frac{p_n}{q_n}$. We can quantify the quality of the approximation by the local irrationality exponent:

$$\left| \rho - \frac{p_n}{q_n} \right| = \frac{1}{q_n^{\mu}} \implies \mu_n = -\frac{\log \left| \rho - \frac{p_n}{q_n} \right|}{\log(q_n)} \tag{8}$$

with $\mu \geq 2$ always when q_n is a partial quotient [13].

Large μ_n (good rational approximations) correspond to trapezoids that are nearly rectangular, with sharply-sloped sides. Such shapes are able to sustain spike formation for many multiples of q_n . The stability of this pattern seems to correspond with how well-approximated ρ is by $\frac{p_n}{q_n}$. Figure 7 shows the pattern for some good approximations. The first, $\left(\rho, \frac{p_n}{q_n}, \mu_n\right) = \left(\pi - 3, \frac{16}{113}, 3.2\right)$, has a pattern that persists for many multiples of $q_n = 113$. The second is $\left(\alpha_{ST}, \frac{40}{81}, 2.8\right)$. We see the pattern break down at $N = 81 \times 14$ - the bottom of the spikes no longer reach the top of the trapezoid.

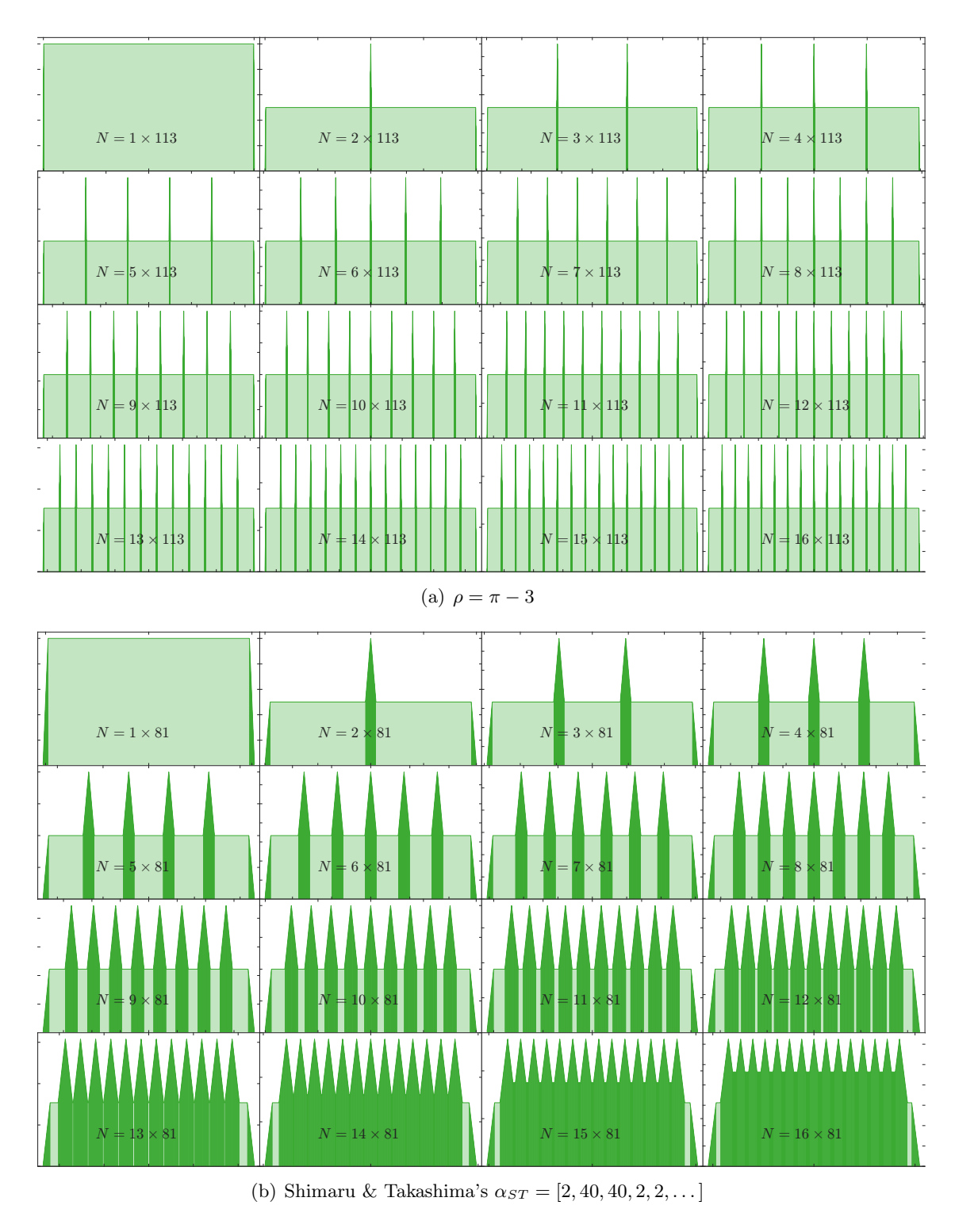


Figure 7: Multiples of partial quotients for two well-approximated irrationals show trapezoids with spike patterns that eventually degrade

Figure 8 shows the pattern for a few irrationals with moderately good rational approximations. We showcase the following combinations of $\left(\rho, \frac{p_n}{q_n}, \mu_n\right)$: The top two rows feature two trancenden-

tals: (top row) $\left(e-2,\frac{51}{71},2.46\right)$, (second row) $\left(\frac{\pi^2}{6}-1,\frac{89}{138},2.42\right)$, while the bottom two rows show-cases some quadratic irrationals $\left([2,2,2,2,10,2,2,\dots],\frac{12}{29},2.71\right)$ and $\left([2,2,2,2,15,2,2,\dots],\frac{12}{29},2.82\right)$. For the first two, the pattern begins to degenerate when k=3, the third when k=4, and the fourth when k=5.

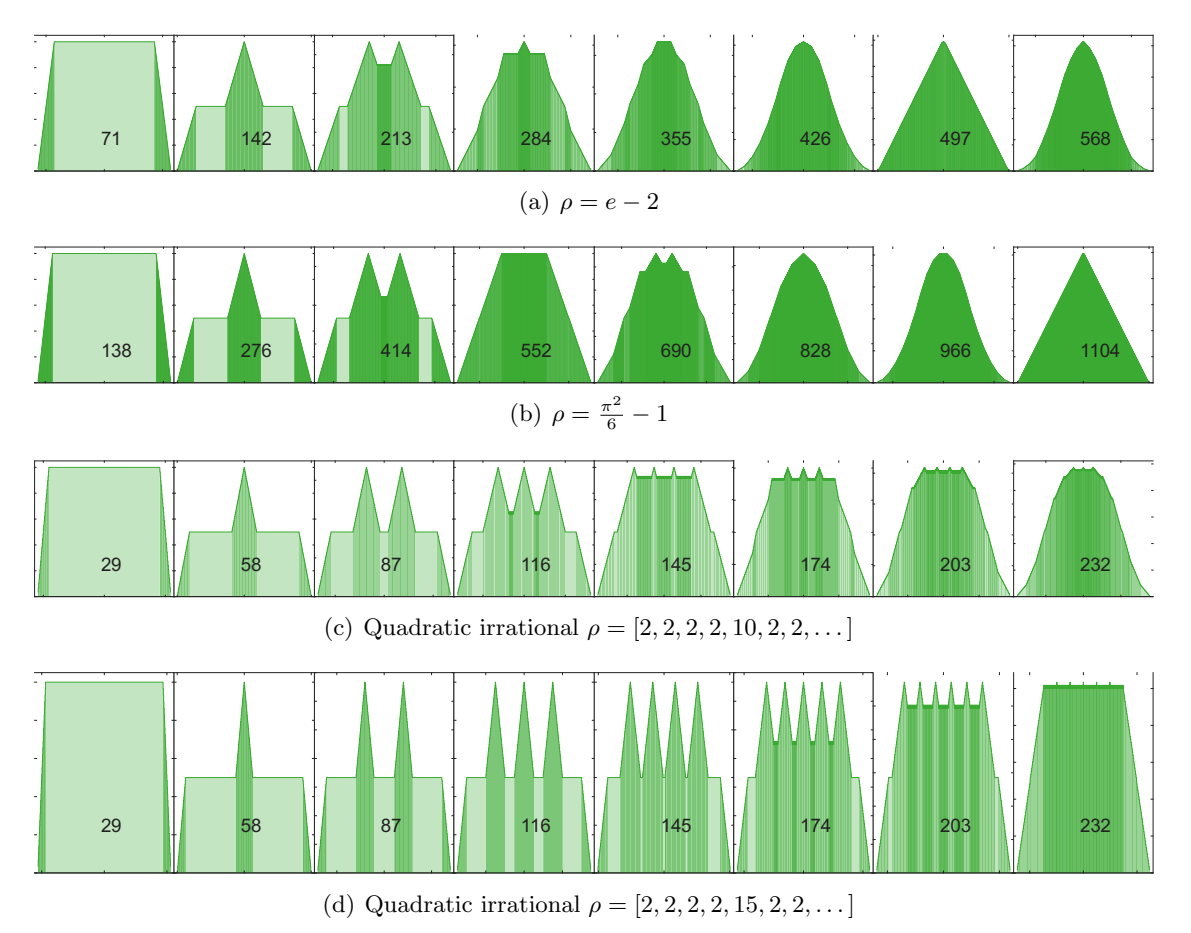


Figure 8: Multiples of partial quotients for some irrationals with moderately good rational approximations show the spike structure start to degenerate early, at k=3 for $\rho=e-2$ and $\rho=\frac{\pi^2}{6}-1$, k=4 for $\rho=[2,2,2,2,10,2,2,\ldots]$, and k=5 for $\rho=[2,2,2,2,15,2,2,\ldots]$

When μ is small (bad rational approximations), the trapezoid is a narrower, pyramid-like distribution unable to support the pattern for k > 1. Some examples are shown in Figure 9.

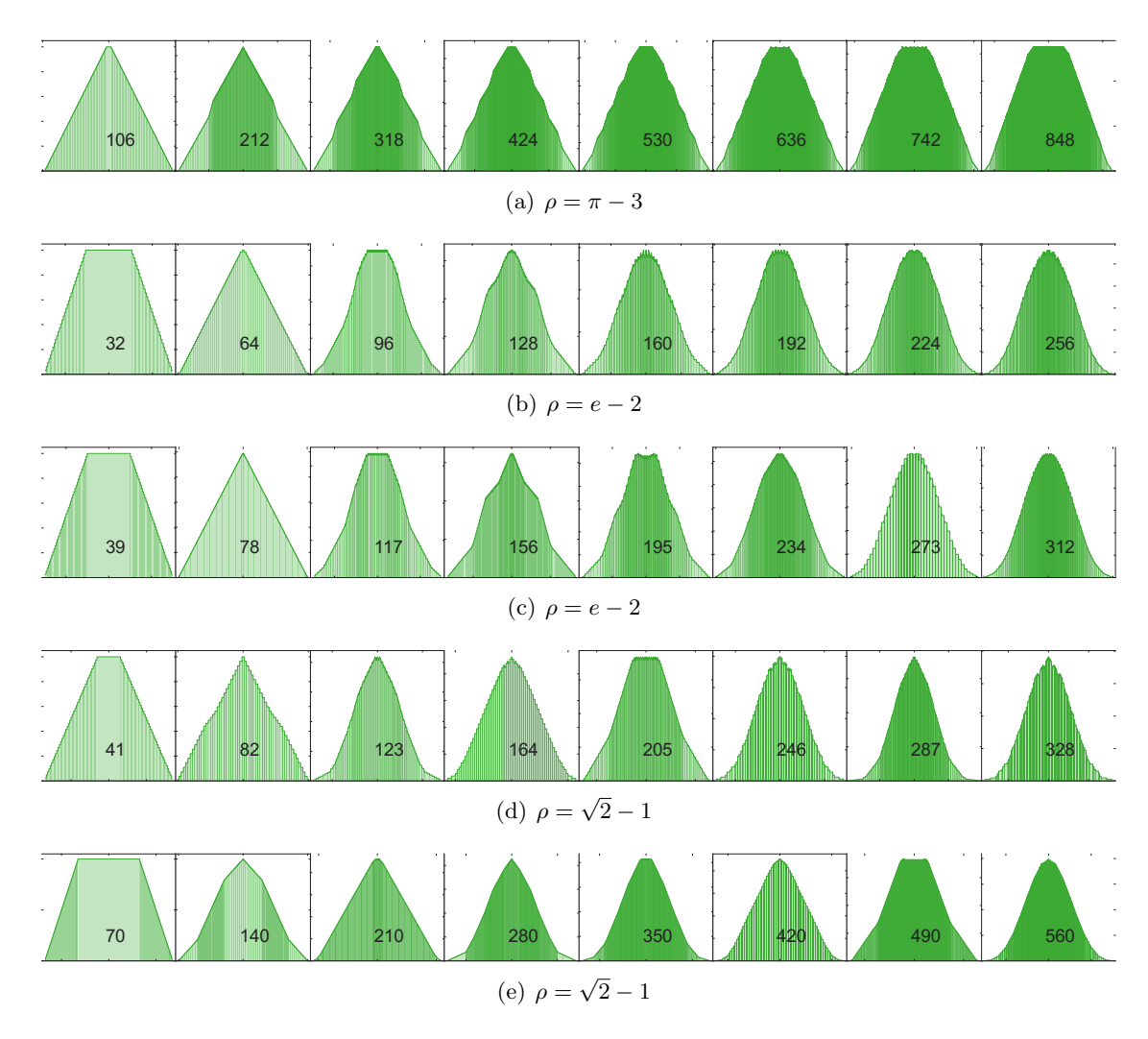


Figure 9: Multiples of partial quotients for some irrationals with bad rational approximations varied behavior.

5 Conclusion

We have presented an algorithm for the computational analysis of the discrepancy of the irrational rotation, $D_N(x,\rho)$. This algorithm allows rapid generation of figures that are guaranteed accurate at machine precision. By defining the structure of the sum through its discontinuities, we are able to bypass both numerical instabilities and computational bottlenecks. We showed that by using a novel discontinuity-tracking algorithm, we can fully characterize the structure of D_N in O(N) time. This enables the rapid computation of its corresponding probability density function pdf and its associated statistical properties (support, variance, and kurtosis) in $O(N \log N)$ time, which allows, for the first time, rapid experimental study of D_N .

We presented two examples of analyses made possible by the algorithm. First, exact plots of Supp(pdf) as a function of N reveal intricate self-similar patterns related to the quotients of consecutive convergents. This framework can be iterated in various ways for example, particular subsequences, rolling extrema, approximations of limits superior and inferior, the shape of the hills, the pre-image of $||D_N||_{\infty}$, and the relationship between support, variance, and kurtosis.

We also presented computational evidence for a recurring pattern in the pdf: when $N=kq_n$ and $\frac{p_n}{q_n}$ is a good approximation for ρ , a predictable spiked-trapezoidal pattern emerges and eventually degrades. The precise onset of degradation and the threshold value of $\left|\rho-\frac{p_n}{q_n}\right|$ permitting persistence beyond k=1 remain open questions. Many other complex structures emerge as N varies which can also be explored.

5.1 Future work

Numerically, the algorithm can be further refined. As noted in Section 2.2, the distances between consecutive branch endpoints in $D_N(x,\rho)$ take on at most three unique values - the third, if it exists, being the sum of the other two (the three-gap theorem). This property could be exploited to improve both efficiency and accuracy.

The discontinuity tracking methodology developed in this paper can also likely be extended to different types of discrepancy sums,

$$D_N(x,\rho) = \sum_{k=1}^{N} \varphi \circ f(x+k\rho) - NE[\varphi]$$
(9)

where $E[\varphi]$ is the expected value. The resulting structure of $D_N(x,\rho)$ may be leveraged in a similar way. Such extensions would broaden the applicability of the DTA and strengthen its connection to problems at the interface of numerical analysis and dynamical systems.

A Selected statistical plots

Statistical plots are shown for ρ of various Diophantine types for $N=2,3,4\ldots$

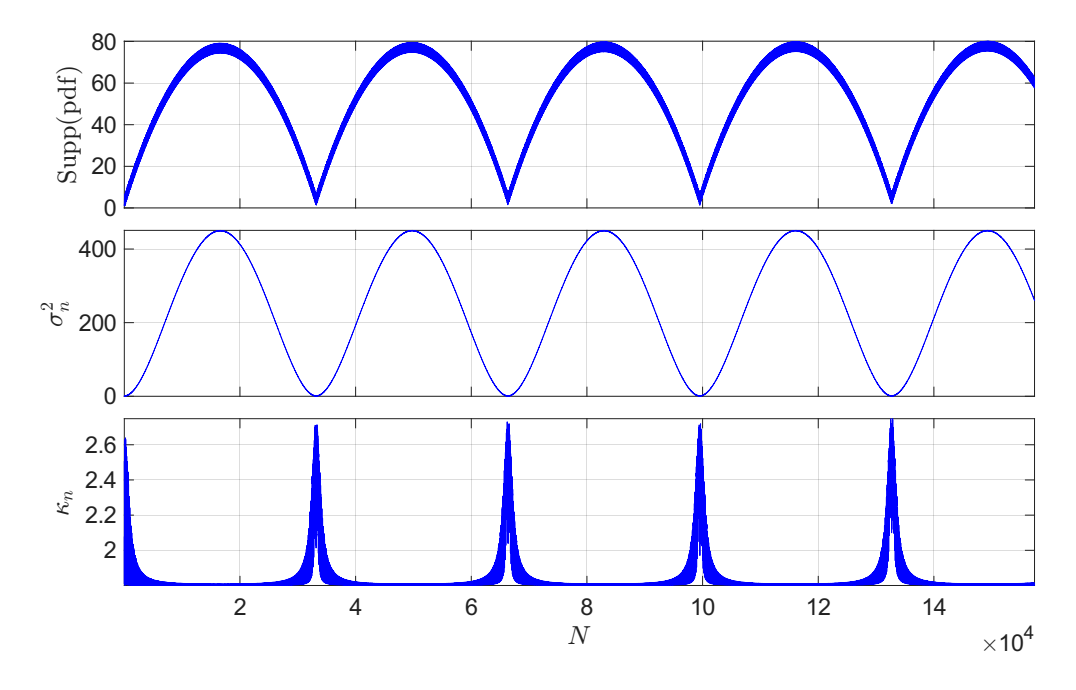


Figure 10: Statistical plots for $\rho = \pi - 3$

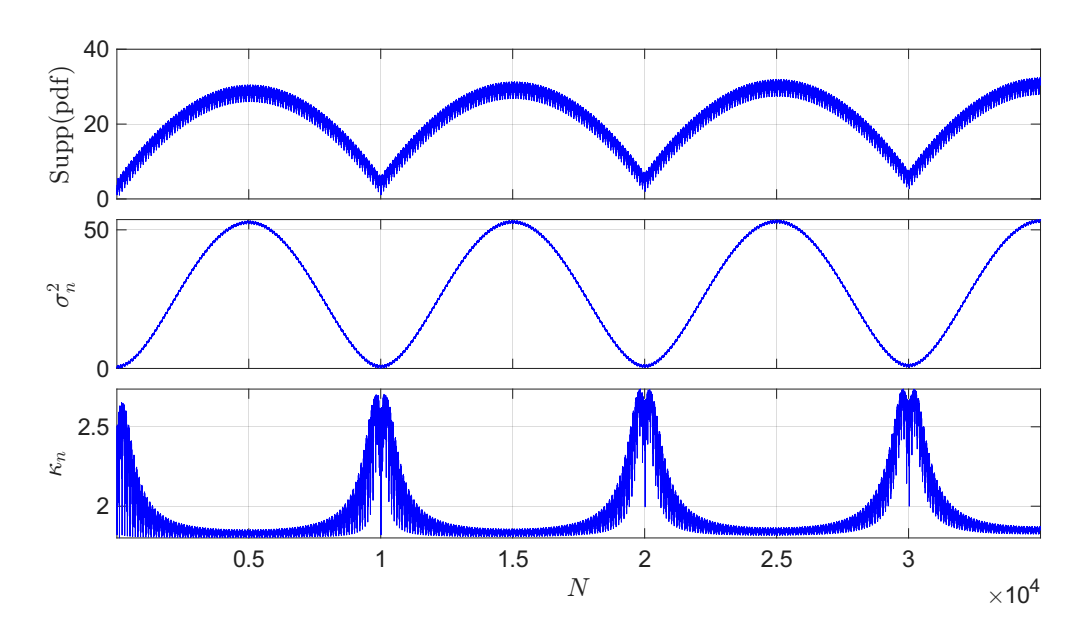


Figure 11: Statistical plots for $\rho=L$

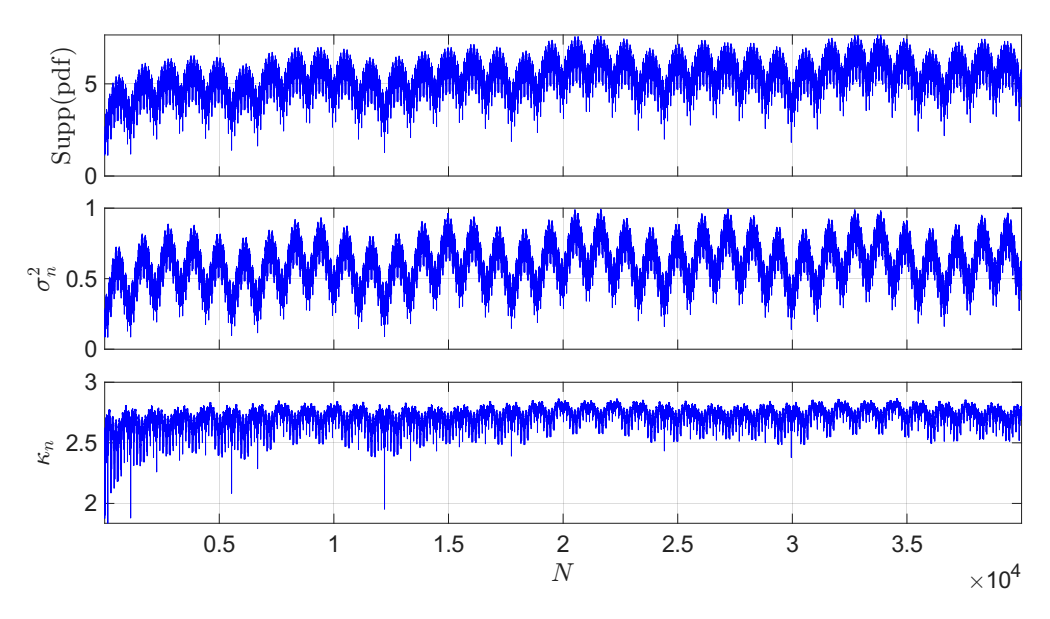


Figure 12: Statistical plots for $\rho = \frac{\pi^2}{6} - 1$

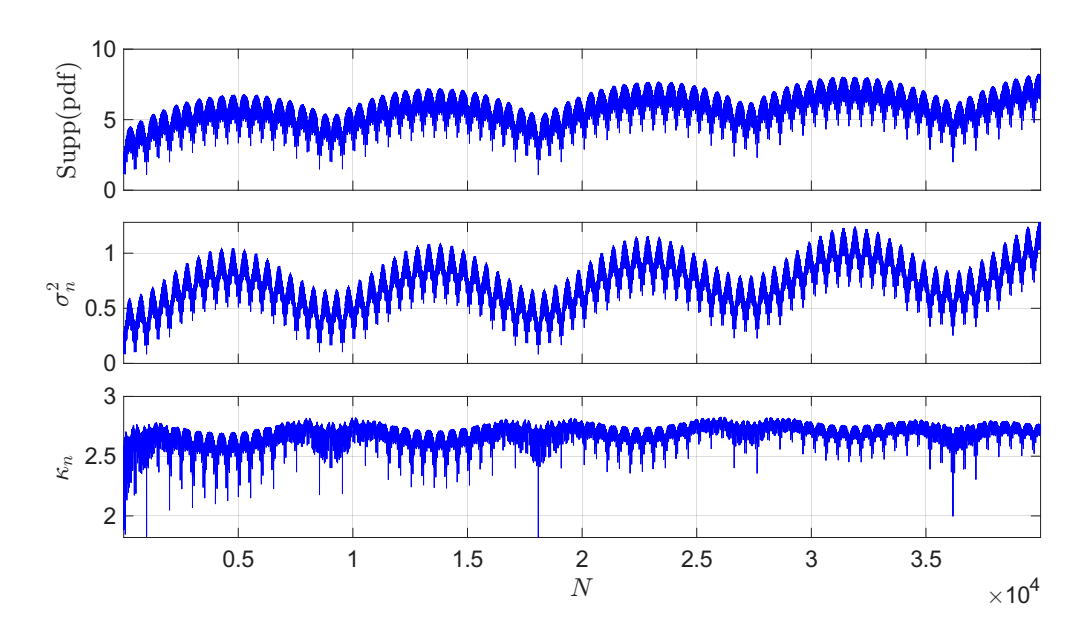


Figure 13: Statistical plots for $\rho = e - 2$

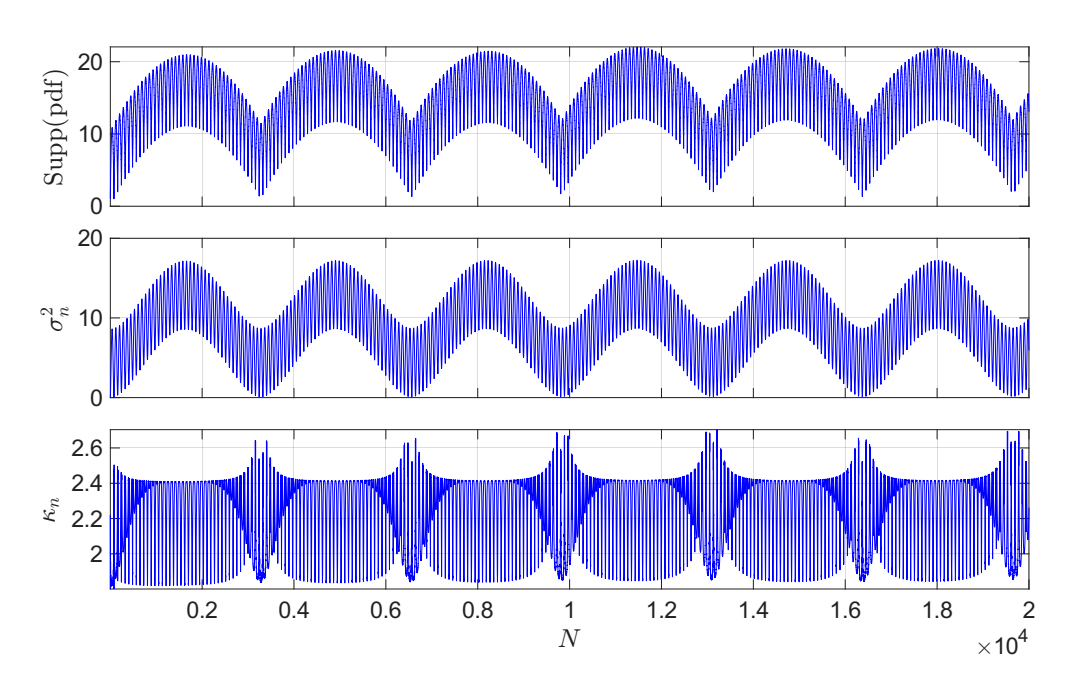


Figure 14: Statistical plots for $\rho = [2, 40, 40, 2, 2, \dots]$

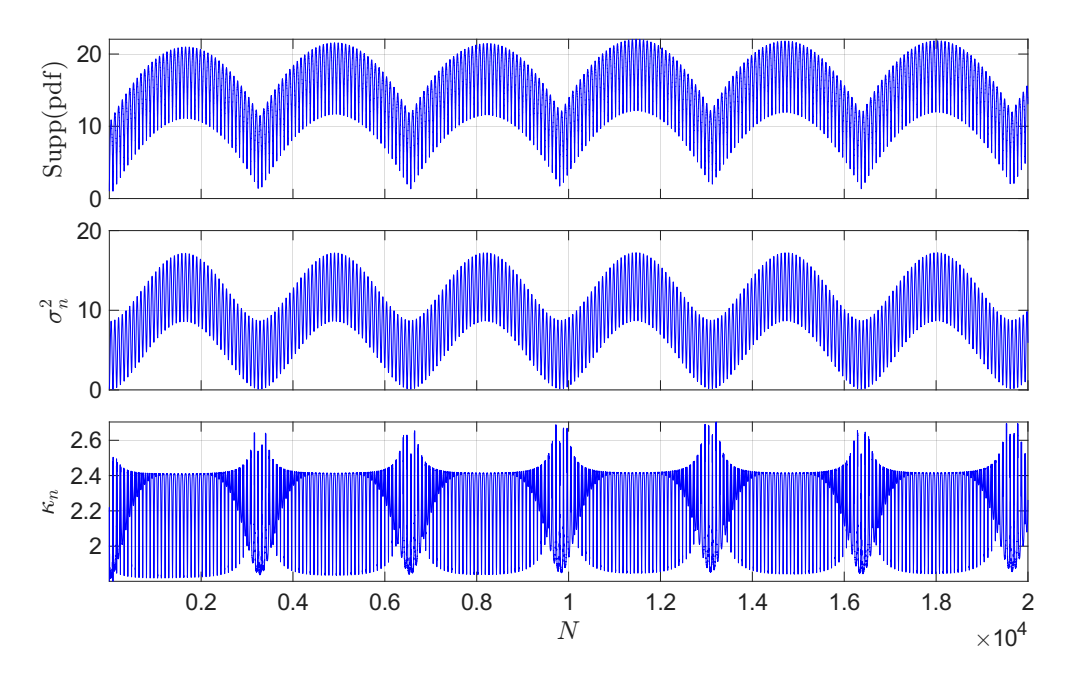


Figure 15: Statistical plots for $\rho = [2, 2, 2, 2, 10, 2, 2, \dots]$

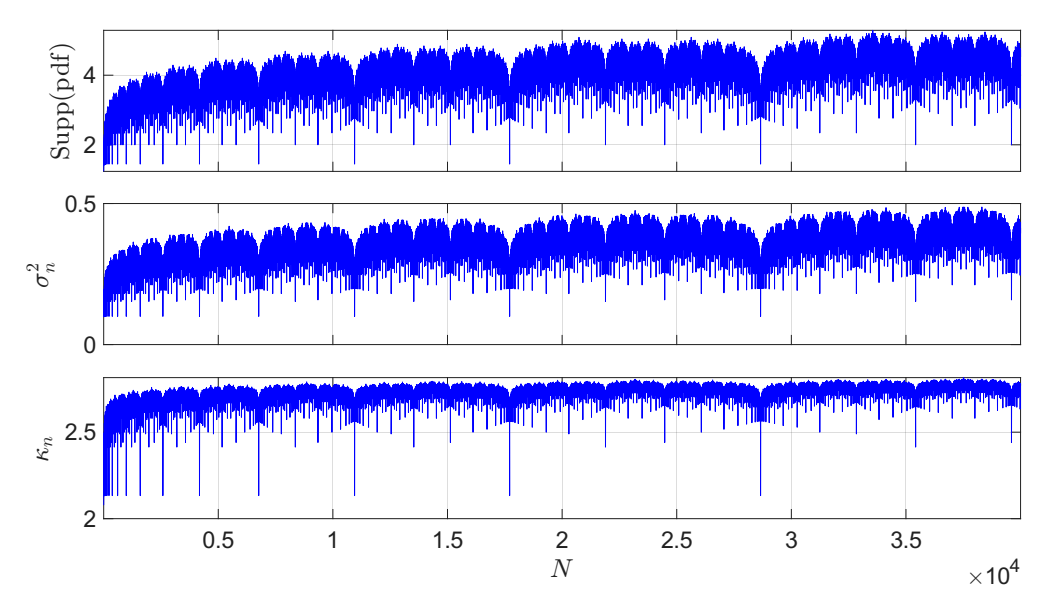


Figure 16: Statistical for $\rho = \frac{\sqrt{5}-1}{2}$

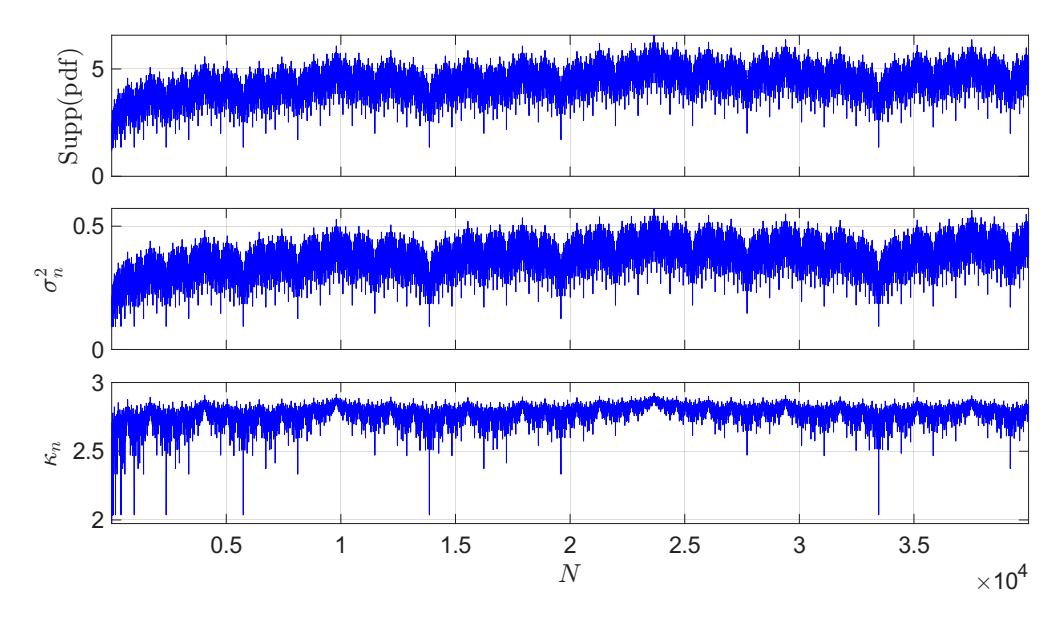


Figure 17: Statistical plots for $\rho = \sqrt{2} - 1$

Acknowledgments

HK thanks CR for proofreading and offering suggestions for improvement.

Code availability

The MATLAB code used to generate the results in this paper is archived at Zenodo and is publicly available at DOI: https://doi.org/10.5281/zenodo.17612959. The repository contains all scripts and instructions necessary to reproduce the figures in the paper.

References

- [1] A. B. Antonevich, A. V. Kochergin, and A. A. Shukur, Behaviour of Birkhoff sums generated by rotations of the circle, Matematicheskii Sbornik, 213 (2022), pp. 891—924, https://doi.org/10.4213/sm9356e.
- [2] G. D. Birkhoff, *Proof of the ergodic theorem*, Proceedings of the National Academy of Sciences, 17 (1931), pp. 656–660, https://doi.org/10.1073/pnas.17.2.656.
- [3] D. Blessing and J. Mireles James, Weighted Birkhoff averages and the parameterization method, SIAM Journal on Applied Dynamical Systems, 23 (2024), pp. 1766–1804, https://doi.org/10.1137/23M1579546.
- [4] A. BOUNTIS, J. J. P. VEERMAN, AND F. VIVALDI, Cauchy distributions for the integrable standard map, Physics Letters A, 384 (2020), p. 126659, https://doi.org/10.1016/j.physleta.2020.126659.
- [5] G. CASELLA AND R. BERGER, Statistical Inference, Chapman and Hall/CRC, 2024, https://doi.org/10.1201/9781003456285.

- [6] A. CUYT, B. VERDONK, S. BECUWE, AND P. KUTERNA, A remarkable example of catastrophic cancellation unraveled, Computing, 66 (2001), pp. 309–320, https://doi.org/10.1007/s006070170028.
- [7] S. DAS, Y. SAIKI, E. SANDER, AND J. A. YORKE, Quasiperiodicity: rotation numbers, in The Foundations of Chaos Revisited: From Poincaré to Recent Advancements, Springer, 2016, pp. 103–118, https://doi.org/10.1007/978-3-319-29701-9_7.
- [8] K. Doi, N. Shimaru, and K. Takashima, An upper estimate for the discrepancy of irrational rotations, Acta Mathematica Hungarica, 152 (2017), pp. 109–113, https://doi.org/10.1007/s10474-017-0702-x.
- [9] K. FUKUYAMA, Metric discrepancy results for geometric progressions with large ratios II, Monatshefte für Mathematik, 202 (2023), pp. 281–315, https://doi.org/https://doi.org/10.1007/s00605-023-01823-4.
- [10] K. FUKUYAMA AND M. YAMASHITA, Metric discrepancy results for geometric progressions with large ratios, Monatshefte für Mathematik, 180 (2016), pp. 731–742, https://doi.org/https://doi.org/10.1007/s00605-015-0791-y.
- [11] A. GONZÁLEZ, À. HARO, AND R. DE LA LLAVE, Efficient and reliable algorithms for the computation of non-twist invariant circles, Foundations of Computational Mathematics, 22 (2022), pp. 791–847, https://doi.org/10.1007/s10208-021-09517-9.
- [12] M. T. Heath, Scientific Computing: An Introductory Survey, Revised Second Edition, SIAM, 2018.
- [13] A. Y. KHINCHIN, Continued Fractions, Phoenix Books, Chicago and London, 1964.
- [14] O. Knill and F. Tangerman, Self-similarity and growth in Birkhoff sums for the golden rotation, Nonlinearity, 24 (2011), p. 3115, https://doi.org/10.1088/0951-7715/24/11/006.
- [15] A. V. Kochergin, On the growth of Birkhoff sums over a rotation of the circle, Mathematical Notes, 113 (2023), pp. 784–793, https://doi.org/10.1134/S0001434623050206.
- [16] L. Kuipers and H. Niederreiter, *Uniform distribution of sequences*, John Wiley & Sons, Inc., 1974.
- [17] B. McKeeman AND L. SHURE, Anadventureofsorts-behind MATLABtech. thescenesofaupgrade, report, MathWorks. Oct 2004. https://www.mathworks.com/company/technical-articles/ an-adventure-of-sortsbehind-the-scenes-of-a-matlab-upgrade.html.
- [18] Y. MORI, N. SHIMARU, AND K. TAKASHIMA, On the distribution of partial sums of irrational rotations, Periodica Mathematica Hungarica, 78 (2019), pp. 88–97, https://doi.org/10.1007/s10998-018-00273-y.
- [19] J. PITMAN, *Probability*, New York: Springer-Verlag, 1993.
- [20] L. RAMSHAW, On the discrepancy of the sequence formed by the multiples of an irrational number, Journal of Number Theory, 13 (1981), pp. 138–175, https://doi.org/10.1016/0022-314X(81)90002-0.

- [21] L. ROÇADAS AND J. SCHOISSENGEIER, On the local discrepancy of (nα)-sequences, Journal of Number Theory, 131 (2011), pp. 1492–1497, https://doi.org/10.1016/j.jnt.2011.01.016.
- [22] J. SCHOISSENGEIER, On the discrepancy of $(n\alpha)$, II, Journal of Number Theory, 24 (1986), pp. 54–64, https://doi.org/0022-314X(86)90057-0.
- [23] R. Sedgewick, *Implementing quicksort programs*, Communications of the ACM, 21 (1978), pp. 847–857, https://doi.org/10.1145/359619.35963.
- [24] T. Setokuchi, On the discrepancy of irrational rotations with isolated large partial quotients: long term effects, Acta Mathematica Hungarica, 147 (2015), pp. 368–385, https://doi.org/10.1007/s10474-015-0563-0.
- [25] T. Setokuchi and K. Takashima, Discrepancies of irrational rotations with isolated large partial quotients, Uniform Distribution Theory, 9 (2014), pp. 31-57. URL: https://pcwww.liv.ac.uk/~karpenk/JournalUDT/vol09/no2/03SetokuchiTakashima.pdf.
- [26] M. I. SHAMOS AND D. HOEY, Geometric intersection problems, in 17th Annual Symposium on Foundations of Computer Science, IEEE, 1976, pp. 208–215, https://doi.org/10.1109/ SFCS.1976.16.
- [27] N. SHIMARU AND K. TAKASHIMA, On discrepancies of irrational rotations: an approach via rational rotation, Periodica Mathematica Hungarica, 75 (2017), pp. 29–35, https://doi.org/10.1007/s10998-016-0164-x.
- [28] N. SHIMARU AND K. TAKASHIMA, On discrepancies of irrational rotations with several large partial quotients, Acta Mathematica Hungarica, 156 (2018), https://doi.org/10.1007/s10474-018-0875-y.
- [29] A. Shutov, Local discrepancies in the problem of fractional parts distribution of a linear function, Russian Mathematics, 61 (2017), pp. 74-82, https://doi.org/10.3103/S1066369X17020098.
- [30] THE MATHWORKS, INC., MATLAB version R2025b, 2025, https://www.mathworks.com.
- [31] T. VAN RAVENSTEIN, The three gap theorem (Steinhaus conjecture), Journal of the Australian Mathematical Society, 45 (1988), pp. 360-370, https://doi.org/10.1017/S1446788700031062.
- [32] J. J. P. VEERMAN, D. RALSTON, F. M. TANGERMAN, AND H. Wu, Birkhoff measures, Birkhoff sums, and discrepancies, 2024, https://web.pdx.edu/~veerman/Discrepancies-Bhoff.pdf. Unrefereed manuscript.
- [33] J. VINSON, Partial sums of ζ (1/2) modulo 1, Experimental Mathematics, 10 (2001), pp. 337–344, https://doi.org/10.1080/10586458.2001.10504454.